ARAI Journal of Mobility Technology
Volume 2 • Issue 2 • April–June, 2022, pp. 220-227
Research Paper
https://doi.org/10.37285/ajmt.1.2.8

# On Using Kriging Response Surface Method for EV Battery Pack Structural Response Prediction and Mass Optimization

**Deepak Sreedhar Kanakandath, Sankha Subhra Jana and Arunkumar Ramakrishnan**

*Battery Durability & Fatigue, Tata Consultancy Services, Creator ITPL, Bangalore, Karnataka, India.*

**ABSTRACT**

Structural response of battery packs in electric vehicles when subjected to road loads is an important factor that decides its performance and life during normal operation. In this paper a kriging response surface model is built using a Design of Experiment (DOE) run dataset to predict structural response and global modal frequency metrics of the battery pack. Using this Response Surface Model (RSM), we can rapidly optimize the battery pack design with respect to structural response and achieve significant mass reduction. This method reduces turnaround times for design optimization in early stages of battery pack design.

**KEYWORDS:** Battery pack, Random vibration response, Kriging method, MDO, Optimization, RESS, Electric Vehicle, Battery pack, Multi-disciplinary optimisation, Mass optimisation, Response surface model, Automotive, CAE, Finite element method.

## Introduction

As the demand for electric vehicles rise, the need for battery packs that provide better driving range as well as enhanced performance also increases. With larger battery packs, the response of the pack to road shocks and vibrations is a key metric that is analyzed to ensure longevity of the pack and safety of the customers. This study considers the use of kriging-based Response Surface Models (RSM) to develop the capability to predict the vibration response of a battery pack, subsequently aiding in mass optimization. Kjell and Lang, 2013 [1] summarizes different battery vibration test standards applicable for Li-ion batteries. The major goals of this study are to:

- Build a response surface model of the battery pack vibration response behavior using Kriging response surface method
- Predict response, global modes, and mass of the battery pack for different component gauge variations using the RSM
- Achieve mass reduction for the battery pack using prediction functions from kriging
- Contribute to Multi-Disciplinary Optimization (MDO) activities using this prediction capability

## Simulation Loads and Considerations

### Battery vibration test standards

Various standards specify test procedures that emulate the effect of sustained road loads on battery modules and packs, which ultimately affect the performance and life of the Rechargeable Energy Storage System (RESS). To perform such test cases, either sine-sweep method or random vibration is used.

**SAE J2380** standard for vibration testing of electric vehicle battery uses road load data measured through 100,000 miles of vehicle operation (Figure 1), which is condensed to a power density spectrum that shows the combined effect of shock loads at various G-levels. The test procedures specified in the document requires a 3-axis shaker table capable of generating accelerations up to 1.9Gs, over a frequency range of 10 to 200Hz as per SAE J2380, 2013 [2].

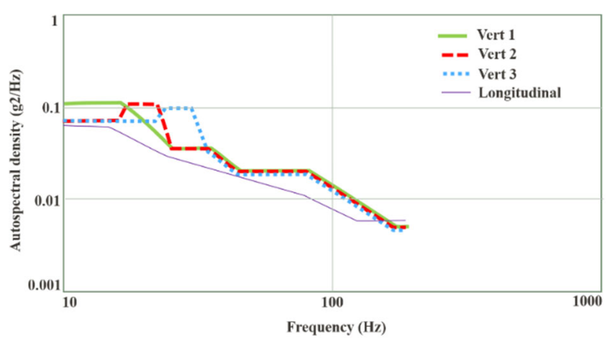


**Fig. 1.** SAEJ2380 random vibration spectra.

During the test, the battery is checked for loss of electrical isolation, resonance conditions, voltage fluctuations as well as thermal failure conditions. The manufacturer can include further measurements for compliance with their additional requirements. Overall, the tests ensure compliance of the battery structural and performance integrity to road-load conditions for a vibration profile up to standard response $G_{rms}$ targets. **USABC procedure #10** specifies similar requirements for random vibration tests, with an added provision for sine-sweep. The sine-sweep excitation is applied at the vehicle resonant frequency, specified by the U.S. Advanced Battery Consortium (USABC) within the range from 10Hz to 30 Hz, as per USABC, 1996 [3]

The test standards serve as guidelines for studying the structural response of a battery pack. A battery module that is compliant with these standards would perform nominally at input vibration levels less than maximum specified in the test standard. Hence, we should ensure that the same levels feed into the mechanical hold down locations for the modules (say bolting regions), ensuring pack life and consistent battery performance over expected road load conditions.

### RLDA & vRLDA road profile input

Road Load Data Acquisition (RLDA) is a method used to measure vehicle response in chosen driving environments. Hooper and Marco, 2014 [4] explains battery pack vibration measurement instrumentation and road surface classifications. The measured data is a result of monitoring important parameters that affect vehicle driving performance such as air and tire resistance and rolling speed. RLDA generates large amounts of data that is compressed into a Power Spectral Density (PSD) profile, which gives an overview of the shock load intensities over a frequency spectrum.

Schudt et al. , 2011 [5] demonstrates the Virtual Road Load Data Acquisition (vRLDA) capability that is leveraged to generate virtual road load data well ahead of any tangible hardware build. Since measured data is seldom available for Battery Electric Vehicles (BEVs), it is a common practice to use road profile data from generic cars or trucks along with vRLDA data to form a derived curve that is assumed to have close conformance with actual vehicle road load response behavior. This input profile curve is used to analyze the structural response of the pack.

### Vibration response simulation in FEA

Simulation of structural response is conducted using a CAE solver with the selected PSD profile input. The Finite element (FE) model of the battery pack is solved to figure out the modal frequencies and vibration response to generate peak response results in $G_{rms}$ at the regions where the modules are connected to the battery pack enclosure (Figure 2). The RESS to vehicle attachment points are constrained.

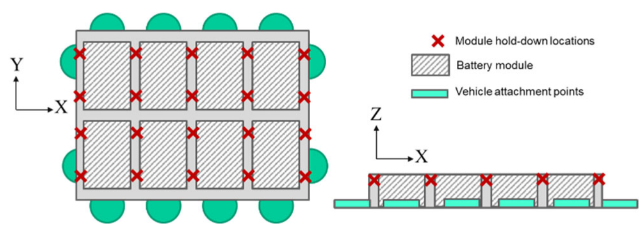


**Fig. 2.** Representation of the battery pack model.

Performance targets are specified based on the ability of the battery module to retain structural and operational integrity. If the $G_{rms}$ response levels measured at the connection location (Figure 3) is greater than the target value it is tested for using any of the mentioned standards (decided based on standards and manufacturer preferences), the analysis is concluded a failure. However, in our study, the battery pack is already compliant to standard targets, and we aim at reducing mass from the structure to optimize it further.

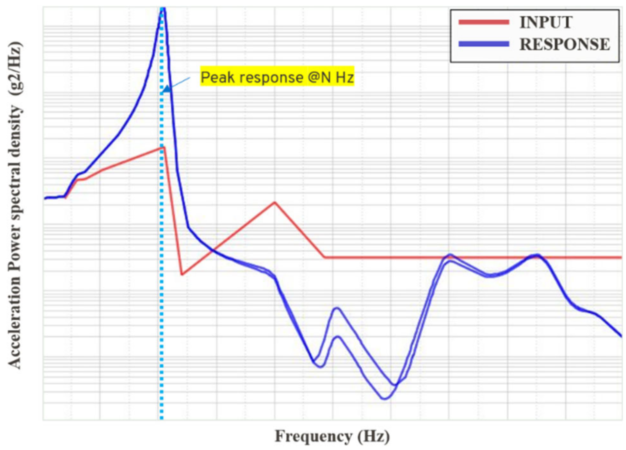


**Fig. 3.** Output Acc (Y) vs Frequency (x) response curve at a measured point (module hold-down location).

Besides the peak response targets, the first three global frequency modes of the battery pack are also recorded to ensure that it is sufficiently displaced from the dominant vehicle resonant frequency.

## Response Surface Modelling

The main goal of this study is to predict the structural response of a battery pack instantaneously without running recurring simulations to support MDO activities. Rather than running multiple analysis to validate each optimized battery pack FE configuration, a Low Fidelity Model (LFM), otherwise known as a metamodel is created as an RSM that can predict a similar result in a less computationally intensive way, as explained by Martin and Simpson, 2004 [6]. Creating the LFM requires data samples from reality, and in our case the reality is substituted by a High-Fidelity Model (HFM) which is the Finite Element Analysis method used for response simulation. To sample data from various sites, we run a Design of Experiments (DOE) procedure, to generate multiple input FE models. To fit the metamodel, a Kriging surface method is used.

### Kriging method

The Kriging method is a statistical interpolation technique, consisting of a parametric regression model and a nonparametric stochastic model. The stochastic parameters are defined using design of experiments (DOE) data obtained here by solving FE models generated according to a generated DOE matrix, explained in Zhaoyan et al., 2015 [7]. This method finds its origins in Geostatistics, pioneered by a South African mining Engineer named Danie G. Krige. Kriging was used to model underground mineral concentrations using data from just a few core drill samples.

The method can accomplish response prediction at any point, as well as assess the local uncertainty called Kriging variance on the response. Magnitude of variance determines certainty of the prediction.

In traditional multi-order regression fits, the form of the curve is assumed early before the fitting is done. Kriging considers outputs of a system as a random process and is comprised of two parts: A linear regression component that projects the general trend of the data, and a probabilistic component that estimates the deviation from measured data. [[7]].

[[7]] $\hat{y}(x) = \boldsymbol{f}^{T}(x)\boldsymbol{\beta} + Z(x)$

The stochastic component in kriging, denoted by Z(x), assumes that the errors in predicted values at interpolation locations must always be a Gaussian distribution (Figure 4). Discussion regarding selection of kriging form (choice of Spatial correlation function (SCF)) and using univariate SCF for each input dimension is explained in [[7]].

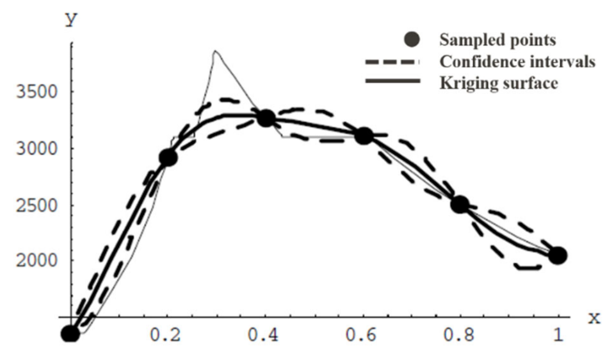


**Fig. 4.** Example of a kriging model. Dotted lines indicate confidence intervals.

Various research material is available for application of Kriging methodology in CAE optimization in finite element models. Dong et. al, 2019 [9] demonstrates the use of Kriging based optimization in the design of the hull-structure of an autonomous underwater vehicle. Finite element models are run to find the maximum von-mises stress, buckling load of the shell structure, and the sample values are used to build the response surface model. Kachinowski and Fu, 2005 [8] shares information about a Kriging-based error reduction approach used in vehicle occupant restraint system design, in vehicle structure CAE. In this study, we generate and solve multiple DOE models from a baseline battery pack model to create an output dataset. The kriging method is used to fit RSMs, which are then cross validated with the same input dataset using a "leave-one-out" method. The RSM is then used to predict vibration response for a given configuration of the pack built using controlled component gauges, and possibility of mass optimization is investigated.

**Input parameters for DOE**

A host of input parameters may be chosen to tune with in the battery pack model, such as component gauges, material, parametrized component features etc. These parameters will essentially function as the "knobs" to control for the user to optimize the model once the RSM is generated. In earlier phases of the pack design, the component designs are comparatively crude, and thus simple gauge reduction or material changes are enough to enable optimization studies. Here the input parameters are set as component gauge variations.

The components are grouped into nine different blocks based on baseline gauge values and/or depending on how they are attached to the structure (Figure 5). Gauge blankets are selected based on how much control we require in the system during prediction. All components within a gauge blanket are set to the selected gauge in each DOE model.

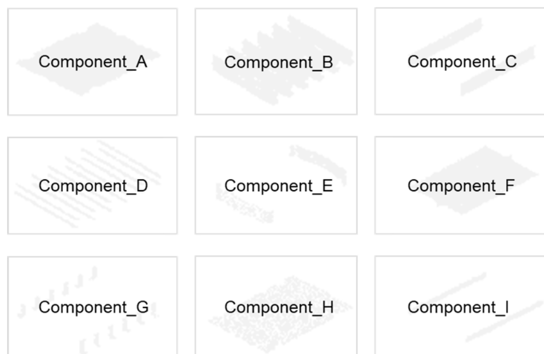


**Fig. 5.** Blanket gauge groups for components.

**DOE matrix**

**Selection of input variable bounds:** The DOE matrix is generated based on user-specified levels of gauges (Table 1), considering the gauge variables as discrete. This would ensure that generated gauges in DOE models do not have unrealistic values that have practical implications in manufacturing. Also, it should be noted that any change in gauge would apply to all components within the group, and it is not possible to vary gauges for specific components in a group once they are assigned to a design variable input. Assigned gauge levels for each variable are shown in table 1.

TABLE 1

DOE input parameters and discrete gauge value levels

| Gauge_blanket | Code | Type | Levels (mm) |
|---|---|---|---|
| Component_A | P1 | Q | 1/1.2/1.4/1.5/1.6/1.7 |
| Component_B | P2 | Q | 0.7/0.8/0.9/1/1.1/1.2 |
| Component_C | P3 | Q | 0.7/0.8/0.9/1/1.1/1.2 |
| Component_D | P4 | Q | 0.7/0.9/1.1/1.2/1.3/1.4 |
| Component_E | P5 | Q | 1.8/1.9/2/2.1/2.2 |
| Component_F | P6 | Q | 1/1.1/1.2/1.3/1.4 |
| Component_G | P7 | Q | 0.8/0.9/1/1.1/1.2 |
| Component_H | P8 | Q | 1/1.2/1.4/1.5/1.6/1.7 |
| Component_I | P9 | Q | 1.5/1.7/1.9/2/2.1/2.2 |

**Experiment design method:** A Strength-Two Orthogonal array design is used to generate the DOE matrix, with the above shown nine input variables. The key feature of this method is that it produces a set of samples that yield uniform sampling in any *t*-dimensional projection of an *n*-dimensional design space where (t<n) as explained by Giunta et al., 2003 [10]. Orthogonal array sampling produces a design sample subset from a library of stored array samples, and a pre-defined number of DOE points are output for use. An example for a 2-strength OA in a 3-dimensional design space is shown in figure 6.

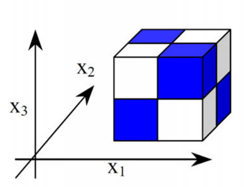


**Fig. 6.** Each of the shaded bins contain one sample. The figure represents a 3-dimensional, 2 strength OA [10]

In this scenario with 9 input variables, 64 DOE points are selected as optimum, below which the correlation value with the full array starts to deteriorate. An example of the generated DOE matrix is shown in table 2.

TABLE 2

DOE points in the generated matrix (all gauges in mm)

| Point | Comp A | Comp B | Comp C | Comp D | Comp E | Comp F | Comp G | Comp H | Comp I |
|---|---|---|---|---|---|---|---|---|---|
| 1 | 1 | 1.2 | 0.8 | 1.1 | 2.2 | 1 | 1.2 | 1 | 2 |
| 2 | 1.7 | 0.7 | 0.8 | 1.4 | 1.8 | 1.3 | 0.8 | 1.6 | 1.7 |
| . | . | . | . | .. | . | . | . | . | . |
| 64 | 1.4 | 0.9 | 0.8 | 1.2 | 1.9 | 1.2 | 0.9 | 1.4 | 1.9 |

Size of the dataset does have an impact on the quality of surface fits, but too many input design variables would require a very large number of DOE runs that will consume excessive computing resources and time. For this problem, 64 DOE models are generated. These 64 models, along with the baseline model are used to generate the RSM.

### Generating FE models using the doe matrix

The CAE preprocessing software Hypermesh™ was used to generate the DOE models in the selected solver format. From the baseline model, the property "PSHELL" cards (Figure 7) are isolated, and the gauge values are fed as a spreadsheet file to a tcl/tk script. This generates and exports all required DOE models to a directory of choice. The files are submitted as batch to an HPC cluster to solve.

```
$HMNAME PROP
1081"XXXXXXXX_001_XXXX_XXXX_FRT_UPR_LH_aa_00mm" 4
$HWCOLOR PROP          1081      11
PSHELL      1081119095100.7     11909510        11909510        0.0
$HMNAME PROP
1083" XXXXXXXX_001_XXXX_XXXX _Bkt_FRT_UPR_bb_00mm" 4
$HWCOLOR PROP          1083      11
PSHELL      1083103042101.2     10304210        10304210        0.0
```

**Fig. 7.** PSHELL property generated by script for DOE models

### Doe results

The out and .pch files after solver modal and response runs are parsed to extract relevant output information to build the RSM model. Python and tcl scripts enable file parsing and result extraction. Global modes are extracted based on effective mass fraction participating in a frequency mode. A certain threshold value of 20%-30% is decided, according to which global modes are extracted from the result file (Figure 8). Generally, frequency modes having less than 20% mass participation would be local modes having no real effect on the battery pack.

| # | Freq | Xt | Yt | Zt | Xr | Yr | Zr |
|---|---|---|---|---|---|---|---|
| 2 | 58.79 | 3.7E-05 | 2.4E-06 | 0.7653 | 2.5E-05 | 0.731 | 2.7E-06 |
| 4 | 64.45 | 0.00044 | 0.02978 | 2.7E-05 | 0.4918 | 0.00022 | 0.02831 |
| 10 | 72.48 | 0.5248 | 0.00067 | 0.00118 | 5.24E-07 | 0.00552 | 0.00066 |
| 53 | 115.4 | 5.23E-08 | 0.4953 | 1.2E-05 | 0.2229 | 8.9E-06 | 0.3907 |

**Fig. 8.** Extracted global modes for a DOE point. Effective mass fractions in each DOF are shown.

Similarly, the peak response value in $G_{rms}$ is also extracted in X (fore-aft), Y (lateral) and Z (vertical) directions, along with the corresponding frequencies. (Figure 9). The mass of each DOE model is directly computed from Hypermesh™ at the time when all the DOE models are initially generated.

| DOE # | Max X | Max Y | Max Z | Freq X | Freq Y | Freq Z |
|---|---|---|---|---|---|---|
| 1 | 1.8 | 0.78 | 0.91 | 76 | 114 | 67 |
| 2 | 1.78 | 0.83 | 1 | 75 | 111 | 62 |
| 3 | 1.87 | 0.79 | 0.87 | 74 | 112 | 65 |
| 4 | 1.79 | 0.77 | 0.84 | 76 | 114 | 68 |
| 5 | 1.86 | 0.79 | 0.92 | 74 | 111 | 64 |
| 6 | 1.8 | 0.81 | 1 | 75 | 112 | 63 |
| 7 | 1.77 | 0.78 | 1.03 | 74 | 113 | 62 |

**Fig. 9.** Extracted response results and corresponding frequencies for the first seven DOE points

## RSM Generation and Cross Validation

To generate a kriging surface, all design variables (gauge buckets 1-9) and result outputs (10 outputs) are used. A general structure of the RSM is summarized in figure 10.

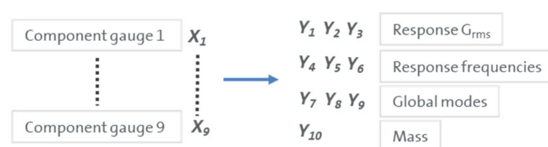


**Fig. 10.** General structure of the RSM used for prediction

The RSM is cross validated using the "leave-one-out" method. Here, the actual value of each point in the DOE space is predicted using a surface comprising of all other points in the space. An ideal case would have all points in the Predicted vs Actual value plots group around the 45-degree line (Figure 11). In this case, the plot for output variable "Freq Y" shows most dispersion, but we may ignore it because our battery pack model shows comparatively mild response conditions in the lateral vehicle direction.

The error vs point number plot (Figure 12) shows the error in prediction for all the 65 DOE points we have selected to generate the RSM. Outlier data points can easily be identified from this plot. Similarly, error plots for all outputs are analyzed.

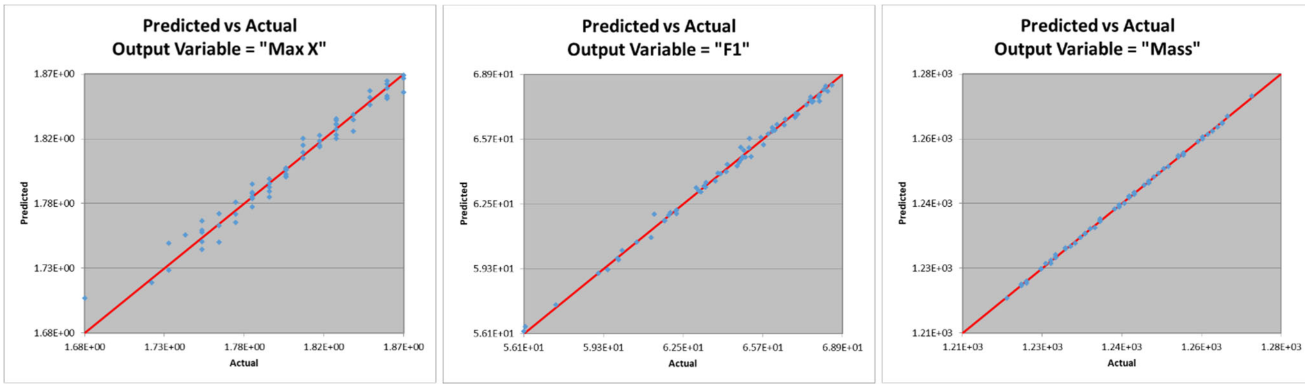


**Fig. 11.** Predicted vs Actual value plots using "leave-one-out" cross validation technique for Max X response, First modal frequency, and Mass.

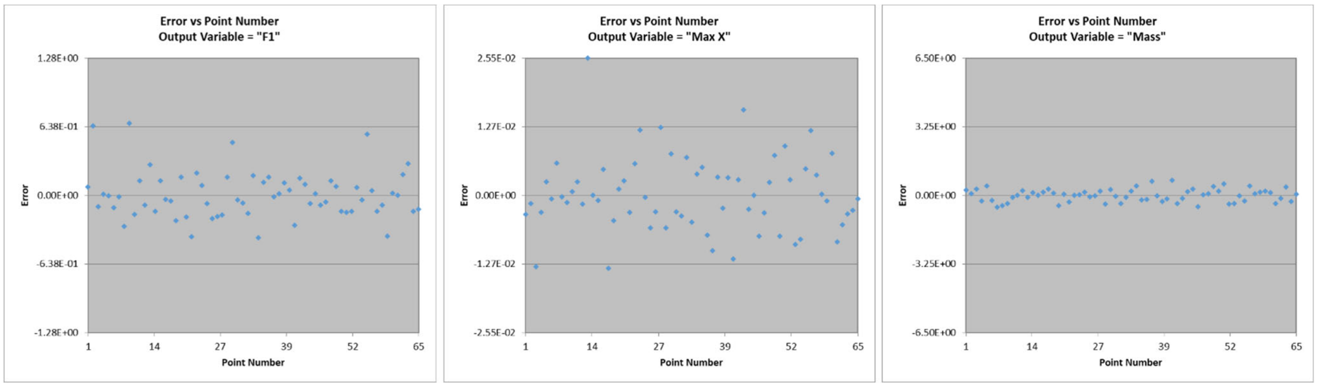


**Fig. 12.** Error vs Point number (DOE) plot for Max X response, First modal frequency, and Mass.

The mean squared errors (Table 3), calculated from variance of output from the regression fit as in Kachnowski, B et al. [[7]], calculated as a fraction of output range are shown below:

TABLE 3

Mean squared errors for outputs after cross validation

| **Output param** | **Param-code** | **Mean squared error as a fraction of Y range (%)** |
|---|---|---|
| Global mode 1 (Hz) | F1 | 1.70 |
| Global mode 2 (Hz) | F2 | 8.08 |
| Global mode 3 (Hz) | F3 | 6.02 |
| Peak response in X ($G_{rms}$) | Max X | 3.68 |
| Peak response in Y ($G_{rms}$) | Max Y | 5.56 |
| Peak response in Z ($G_{rms}$) | Max Z | 1.98 |
| Peak X resp. Frequency (Hz) | Freq X | 5.83 |
| Peak Y resp. Frequency (Hz) | Freq Y | 9.99 |
| Peak Z resp. Frequency (Hz) | Freq Z | 2.68 |
| Mass of battery pack | Mass | 0.46 |

## Analysis of variance (ANOVA)

The analysis of variance studies the influence of inputs parameters on the outputs. By performing ANOVA, we can figure out the percentage contributions of each input parameter for the DOE and effectively tune the model for further optimization.

The design variables P1, P7 and P8 show significant contributions in peak response and first global frequency mode outputs (Figure 13). This knowledge can be used to refine and/or eliminate the design variable inputs in further studies. Convergence analysis gradually adds data points as the model is checked for percent contributions, finally reaching a point where no further addition of points show increase or decrease in percent contributions in an input parameter. This also helps to validate the DOE space size that is used to build the RSM. The convergence chart for one of the output parameters (Max X – Peak response in the X direction) is shown in Figure 14.

When multiple input parameters have an interaction with each other, the effect on changing one parameter on the output differs with the value of the other (Figure 15). Whenever this value is more than 5%, it is plotted as an interaction plot that plots main effect of both parameters when the other is kept constant at its lower or upper bounds. The main effect plot (Figure 16) illustrates the nature of variation of the output when the input parameters are varied from 0% (the lower bound) to 100% (the upper bound). Here, parameter P2 is found to have no effect until it approaches the upper bound value. Except parameters P1, P7 and P8 others are found to have no real significance in predicting value of “Max X”. Although these inferences may not reflect in real life design choices, it can be used to streamline the RSM in future iterations.

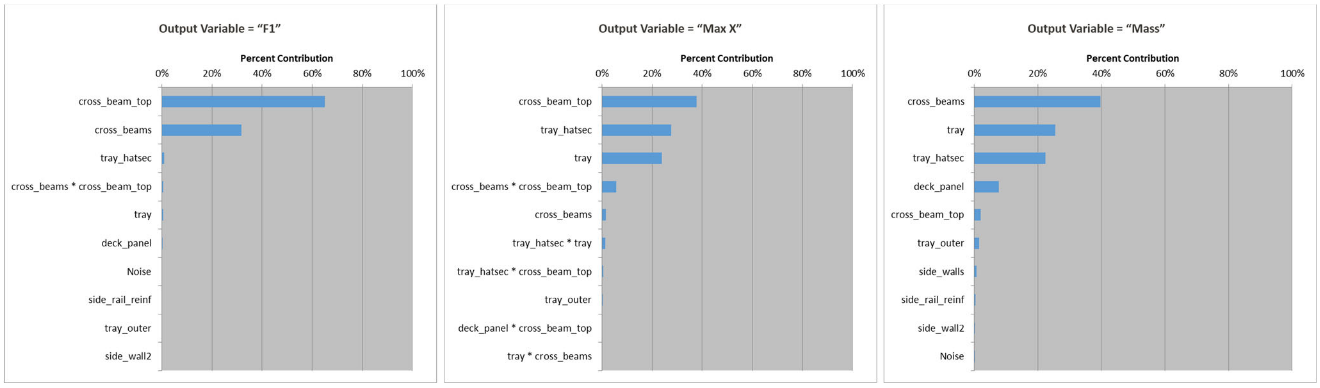


**Fig. 13.** ANOVA percent contributions for input variables P1-P9 and their interactions, for Max X response, First modal frequency, and Mass

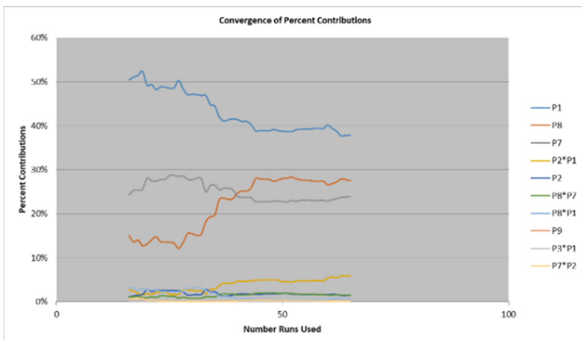


**Fig. 14.** Convergence of percent contributions for output "Max X".

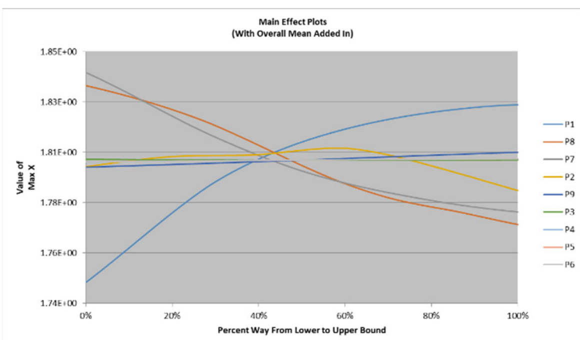


**Fig. 15** Main effect plots for all inputs P1-P2 for output Max response X.

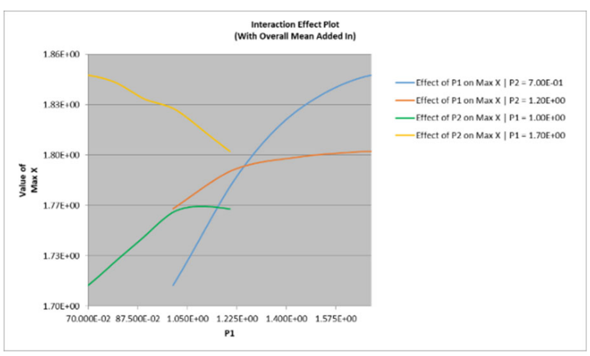


**Fig. 16.** Plot showing interaction between P1 and P2.

Here, increasing gauge of parameter "P2" when "P1" value is kept at its lower bound tends to increase the peak X-response value of the pack, and vice versa when kept at the upper bound. Similarly, it is ideal to analyze all variable interactions for all outputs to gain valuable insight into the RSM characteristics.

## RSM Correlation and Mass Optimization

The Response surface model generated using Kriging method enables export of prediction functions, to a specified confidence level (95%). Prediction functions are generated and exported for each of the ten output/Reponses. Using these functions, a dashboard is generated in excel (Figure 17) where for any user-input value of DVs (Design variables – gauges), all required responses can be predicted instantly. However, as the gauge bounds depart the bounds used for building the RSM (the DOE bounds), the prediction results tend to deviate.

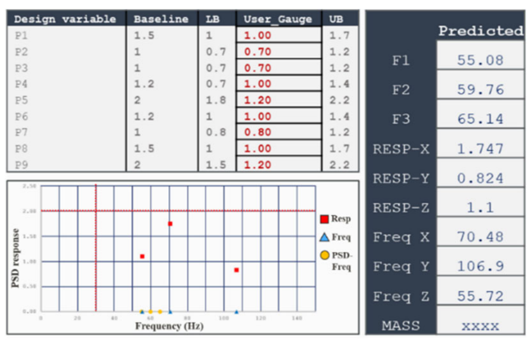


**Fig. 17.** Excel dashboard for response and modal prediction for the battery pack (Sample shown).

Correlation of predicted results are checked by solving FE models with the thickness gauge values used for prediction and comparing the results. Two such sets of gauges are shown in the table below and were selected by were selected on a consensus from relevant stakeholders (Table 4). The difference in results between predicted and FEA outputs are found to match closely, as the cross-validation results also suggested (Table 5).

TABLE 4

Proposed gauge combinations for correlation models

| Gauge_blanket (mm) | Design proposal 1 | Design proposal 2 |
|---|---|---|
| Component_A | 1.00 | 1.00 |
| Component_B | 1.10 | 0.60 |
| Component_C | 0.80 | 0.60 |
| Component_D | 1.20 | 1.20 |
| Component_E | 1.20 | 1.80 |
| Component_F | 1.20 | 1.00 |
| Component_G | 0.90 | 0.80 |
| Component_H | 1.00 | 1.00 |
| Component_I | 1.20 | 1.20 |

TABLE 5

Correlation result data that to show RSM reliability (Mb is mass of the baseline model battery pack)

| Outputs | Proposed gauges #1 | | Proposed gauges #2 | |
|---|---|---|---|---|
| | Prediction | Actual | Prediction | Actual |
| F1 (Hz) | 54.36 | 55.1 | 55.8 | 55.8 |
| F2 (Hz) | 59.19 | 59.9 | 62.62 | 61.8 |
| F3 (Hz) | 63.26 | 69.7 | 74.8 | 71.8 |
| Max X ($G_{rms}$) | 1.7 | 1.76 | 1.72 | 1.7 |
| Max Y ($G_{rms}$) | 0.817 | 0.95 | 0.81 | 0.83 |
| Max Z ($G_{rms}$) | 1.142 | 1.02 | 1.09 | 1.1 |
| Freq X (Hz) | 70.28 | 69 | 71.8 | 72 |
| Freq Y (Hz) | 109.1 | 105 | 111.5 | 108 |
| Freq Z (Hz) | 54.75 | 55 | 55.36 | 56 |
| Mass (Kg) | $M_b$-35 | $M_b$-35 | $M_b$-76 | $M_b$-77 |

A detailed optimization set up may be performed using an established multi-objective optimization technique like the Pareto front, that can quickly generate a set of feasible solutions. This is however a future scope for the study, and mass optimization here is performed through a simple excel data solver that uses outputs from the Kriging RSM predict functions to generate optimum gauge values. The range of optimization may be controlled by varying the thickness bounds (Table 6), provided they do not deviate too much from the DOE bounds.

TABLE 6

Constraints and objectives used for Mass optimization of the battery pack

| Parameter | Type | Objective | Target | Lower bound | Upper bound |
|---|---|---|---|---|---|
| Gauge1-9 | Input | | | Yes | Yes |
| Modal Frequency 1-3 | Output | - | Vehicle modal Target | - | - |
| Response X/Y/Z | Output | - | Target Grms for battery module integrity | - | - |
| Peak response Frequencies X/Y/Z | Output | - | - | - | - |
| Mass | Output | Minimize | - | - | - |

The optimal design obtained within DOE bounds was up to 36kg lesser than the baseline battery pack mass. This mass reduction is a significant result since we can maintain pack modal and road response performances. This prediction interface can now be used in MDO operations as a quick check for estimating modal and response behavior of the battery pack. MDO also involves stakeholders from other CAE disciplines like safety and crash.

## Conclusion

The study conducted here reinforces the use of a metamodel approach using kriging RSM in the design optimization of a battery pack. Since the pack already meets target response requirements, an opportunity is presented for mass reduction using prediction functions of the RSM model. Careful selection of Input design variables that can effectively influence the behavior of the pack are crucial when building the RSM. After generation of the RSM, it is cross validated to ensure model credibility, as well as analysis of variance (ANOVA) is performed to determine if any further streamlining is required while selecting input variables. Multiple gauge proposals were made, and the predicted values were correlated with analysis runs. With the validated RSM, we can quickly predict peak vibration response, global frequency modes as well as mass of the battery pack for ideally all gauge variations of the input parameters. This greatly reduces turnaround time in MDO activities, where validation with respect to modal frequencies and vibration response of the pack are available instantly. This method may be used in the initial stages of the battery pack design when there is maximum room for improvement.

## References

[1] G. Kjell and J. F. Lang, "Comparing different vibration tests proposed for li-ion batteries with vibration measurement in an electric vehicle," 2013 World Electric Vehicle Symposium and Exhibition (EVS27), Barcelona, 2013, pp. 1-11.doi:10.1109/EVS.2013.6914869 http://ieeexplore.ieee.org/stamp/stamp.jsp?tp=&arnumber=6914869&isnumber=6914705

[2] Surface vehicle recommended practice, "SAE standard J2380 - Vibration testing of Electric Vehicle Batteries", issued 1998-01, revised 2013-12, Superseding J2380 MAR2009 https://saemobilus.sae.org/content/J2380_201312/

[3] USABC Electric Vehicle Battery Test Procedures Manual, Revision 2, January 1996. Report No.DOE/ID-10479, Rev. 2. http://avt.inl.gov/energy_storage_lib.shtml

[4] Hooper, James & Marco, James. (2014). Characterizing the in-vehicle vibration inputs to the high voltage battery of an electric vehicle. Journal of Power Sources. 245. 510-519. http://dx.doi.org/10.1016/j.jpowsour.2013.06.150

[5] Schudt, J., Kodali, R., Shah, M., and Babiak, G., "Virtual Road Load Data Acquisition in Practice

at General Motors," SAE Technical Paper 2011-01-0025, 2011, https://doi.org/10.4271/2011-01-0025.

[6] Martin, J. and Simpson, T., "On Using Kriging Models as Probabilistic Models in Design," SAE Technical Paper 2004-01-0430, 2004, https://doi.org/10.4271/2004-01-0430.

[7] Zhaoyan Lv, Zhenzhou Lu, Pan Wang, A new learning function for Kriging and its applications to solve reliability problems in engineering, Computers & Mathematics with Applications, Volume 70, Issue 5, 2015, Pages 1182-1197, ISSN 0898-1221, https://doi.org/10.1016/j.camwa.2015.07.004

[8] Kachnowski, B. and Fu, Y., "Experience with Response Surface Methods for Occupant Restraint System Design," SAE Technical Paper 2005-01-1306, 2005, https://doi.org/10.4271/2005-01-1306

[9] Dong H, Song B, Wang P. Kriging-based optimization design for a new style shell with black box constraints. Journal of Algorithms & Computational Technology. September 2017:234-245. doi:10.1177/1748301817709601

[10] Giunta, A. & Wojtkiewicz, Steven & Eldred, Michael. (2003). Overview of modern design of experiments methods for computational simulations. AIAA. 0649. 10.2514/6.2003-649. https://arc.aiaa.org/doi/10.2514/6.2003-649

Address correspondence to *Mr. Deepak Sreedhar Kanakandath, Senior CAE Engineer, Battery Durability & Fatigue, Tata Consultancy Services, Creator ITPL, Bangalore, Karnataka, India*
Email: deepaksreedhar.k@tcs.com
Phone: 08867016122